Ernst & Sohn
A Wiley Brand

Call for Papers

Civil Engineering Design is an international journal providing innovative theoretical, numerical and experimental methods for current and newly developed building materials like concrete, steel, aluminum, glass, timber, masonry, composite materials and for all aspects of conceptional, structural and performance-based design, experimental testing and numerical modelling including construction, maintenance and demolition for the entire life-cycle of structures. This is completed by the inclusion of geotechnical engineering and soil mechanics from the perspective of structural engineering.

- **Online only, hybrid open-access journal**
- English language, 6 issues per year
- Interdisciplinary and material-independent approach
- Focussed on scientific publications
- Short review and publication times
- Manuscript submission via *ScholarOne*
- Peer-reviewed

You are invited to actively participate in the launch of this new journal, shape it and determine its direction.

Submissions: **https://mc.manuscriptcentral.com/cend**

www.ernst-und-sohn.de/en/cend

Received: 5 April 2019 | Revised: 3 July 2019 | Accepted: 10 July 2019

DOI: 10.1002/cend.201900010

FULL PAPER

Ernst & Sohn
A Wiley Brand

Multiaxial and variable amplitude fatigue of concrete

Peter Heek[1] | Peter Mark[2]

[1]HOCHTIEF Engineering GmbH, Consult Infrastructure, Essen, Germany

[2]Ruhr-Universität Bochum, Lehrstuhl für Massivbau, Bochum, Germany

Correspondence
Peter Heek, HOCHTIEF Engineering GmbH, Consult Infrastructure Alfredstraße 236, 45133 Essen, Germany.
Email: peter.heek@hochtief.de

Abstract

Concrete structures are often exposed to cyclic loads induced by traffic or machine vibrations. To assess fatigue lifes, SN curves serve, which are usually validated by experiments. During testing, reference specimens are exposed to uniaxial and constant amplitude fatigue. However, under real operating conditions loads occur multiaxially and with alternating amplitude and frequency. Thus, the progressively increasing material damage has to be mathematically captured. In this regard, Palmgren-Miner's linear accumulation rule is well established, although it neglects distinct sequence effects. In the article, the SN concept is first extended to multiaxial stress states by introducing an equivalent stress under the notion of isotropic damage. Then, a modified damage accumulation procedure is developed taking into account effects of loading and unloading on residual numbers of cycles to failure in multistage loading processes. The new approach is verified to experimental data taken from the literature and elaborated to a design chart. An example demonstrates the practical application.

KEYWORDS

fatigue, multiaxial and multistage loadings, SN curves, equivalent stress, accumulation of damage

1 | INTRODUCTION

The fatigue behavior of concrete is usually investigated experimentally. In so called Wöhler tests, material samples are subjected to cyclic loads of constant frequency f with maximum and minimum fatigue stresses σ_{max} and σ_{min} to derive numbers of cycles to failure N^{f1}. The fatigue lifes are then related to the corresponding stress conditions and graphically summarized in Wöhler or SN diagrams. Figure 1 exemplarily shows such SN curves for plain concrete with normalized actions in form of stress level $0 < S < 1$ and stress ratio $-1 < R < 1$. According to Equation (1), the stress level relates σ_{max} to the concrete's static strength f_{stat}. R covers the ratio of the minimum and maximum fatigue stresses and thus comprises pulsating stresses ($R > 0$) as well as stress reversals ($R < 0$).

$$S = \frac{\sigma_{max}}{f_{stat}} \tag{1}$$

$$R = \frac{\sigma_{min}}{\sigma_{max}} \tag{2}$$

Obviously, fatigue lifes increase with decreasing stress level and increasing stress ratio.[2–5] Thus, stress reversals are more degrading then pulsating stresses.[6,7] Besides, increasing the loading frequency within the quasi-static domain ($f < 20$ Hz) goes along with enhanced numbers of cycles to failure by trend. However, the frequency effect strongly depends on the loading magnitude and gradually reduces with stress levels.[3,8,9] Effects of the loading type on fatigue lifes due to centric, eccentric, compressive or tensile actions are sufficiently considered by S, if f_{stat} represents an associated strength.[2,3] Thus, different loading types can be treated conceptunally equal.

Test results from the literature advice to extend the SN approach to multiaxial stress conditions as well. Enhanced fatigue lifes in biaxial compression compared with the uniaxial state fit well to corresponding

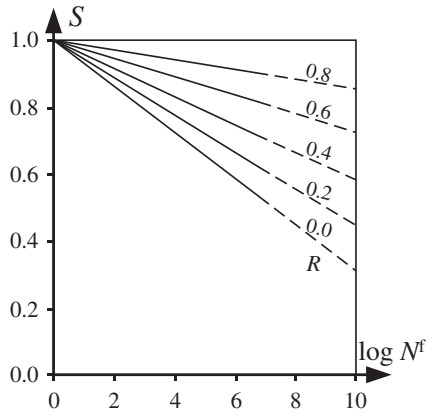

FIGURE 1 Example of SN curves for plain concrete according to Ref. 2

ratios of the static strengths.[10] Moreover, multiaxial tensile loads do not significantly affect the numbers of cycles to failure compared with the uniaxial case,[11] which can be traced back to the correspondence of multiaxial and uniaxial static tensile strengths. Subsequently, the findings are used to generalize well-established SN curves to muliaxial stress conditions. For this purpose, an equivalent stress is introduced.

2 | SN CURVES FOR CONCRETE

2.1 | Literature approaches

A huge number of SN curves for uniaxially stressed concrete are available in the literature, which are either linear[5], multilinear[4], or nonlinear[12] and mainly differ in the descending slope and the involved parameters. In addition to stress level and ratio, the stress amplitude $\sigma_a = 0.5(\sigma_{max} - \sigma_{min})$, the frequency or load duration $T = 1/f$ and the rate-dependent concrete strength f_{dyn} are taken into account.

According to Refs. [7,13], the influence of the loading frequency on N^f can be attributed to the rate-dependent concrete strength in the quasi-static domain, so that f_{dyn} serves as reference strength to calculate dynamic stress levels S_{dyn} analogous to Equation (1). Thereby, very low[14] and very high[15] loading velocities are excluded, as they lead to further degradation effects, either due to the long term load duration or nonlinear temperature gradients induced by internal friction. A transformation between both, Equations (1) and (3) and thus static to rate-dependent formulations, is enabled by the ratio of f_{stat} to f_{dyn}. For the sake of simplicity, the two strength values represent here both, tensile (f_t) and compressive (f_c) components.

$$S_{dyn} = \frac{\sigma_{max}}{f_{dyn}} = \frac{\sigma_{max}}{f_{stat} \cdot \left[\frac{\Delta\sigma}{\dot{\sigma}_0} \cdot f \cdot \alpha_{F-t}\right]^c} = \frac{S}{\left[\frac{\dot{\sigma}_m}{\dot{\sigma}_0}\right]^c} \quad (3)$$

In Equation (3), $\Delta\sigma = \sigma_{max} - \sigma_{min}$ describes the stress difference, $\dot{\sigma}_0 = 1$ N/(mm^{2}s) a reference stress velocity and α_{F-t} a coefficient related to the waveform. Assuming mean stress velocities $\dot{\sigma}_m$, α_{F-t} approximately follows to $\alpha_{F-t} = 1$ for rectangular and $\alpha_{F-t} = 2$ for triangular or sinusoidal waveforms.[13,16] For $\dot{\sigma}_m = \Delta\sigma \cdot f \cdot \alpha_{F-t} < 10^5$ N/(mm^2 s) and thus the quasi-static domain the exponent c can be set to $c = 0.0158$ in dependence on Ref. 17.

The rate-dependent SN approach has originally been developed in Refs. [7,13] for plain concrete (PC) and is taken up in Ref. 18 to be extended to steel fiber reinforced concrete (SFRC). For this purpose, a stress and ductility dependent toughness index α with $0 < \alpha(\sigma_{max}) < 1$ is introduced. In case of brittle PC or SFRC, low values of α close to zero result. A high material ductility, for example, due to the fiber's strengthening effect, yields to enlarged values near one. The dimensionless toughness index is determined by integrating normalized stress-strain relations. For this purpose, stress-strain curves $\sigma(\varepsilon)$ serve in the uncracked state while softening after cracking is gathered via stress-crack width relations $\sigma(w)$. Taking benefit of the analogy between the static and cyclic load-deformation behavior captured by the envelope concept,[3,8] the material response is integrated from zero up to the deformation assigned to the maximum fatigue stress on the descending branch of the postcracking curve.[18] The shape of the underlying $\sigma(w)$ relation is strongly governed by the fracture (tension) or crushing (compression) energy G_f or G_c, respectively. The fracture-mechanical material parameter $G_i = \int_0^w \sigma(w)dw$ with i = c, f denotes the energy per unit area that is dissipated for a complete separation of two crack bands.[19–21] G_i thus corresponds to the total area under the stress-crack width relation. In Ref. 17, G_f is given as a function of the concrete's maximum grain diameter d_g and the compressive strength f_c. It applies to:

$$G_f = G_{f0} \cdot (f_c/f_{c0})^{0,7} \text{ with } fc_0 = 10\,\text{N/mm}^2 \quad (4)$$

d_g (mm)	G_{f0} (N/m)
8	25
16	30
32	38

As f_c is related to a reference strength f_{c0}, various concrete strengths can be treated in an analogous way by Equation (4). G_c is about three orders of magnitude above G_f and varies within the limits of about $10 < G_c < 50$ N/mm.[22,23]

Figure 2 graphically summarizes results of calculated thoughness indexes using the example of a normal strength concrete C 30/37. As expected, large values α occur at low stress levels S and with increasing deformation energy, that is, with increasingly ductile load-bearing behavior.[16]

As evaluations of literature data in Ref. 16 prove a strong correlation between the material's toughness and fatigue lifes, a mathematical relation between N^f and S_{dyn}, R and α is derived in Ref. 18. Multiple regression analysis of $n = 567$ individual test data yield to the following equation with two empirically derived regression coefficients $(\sqrt{103}; \frac{\pi}{2})$ ahead the two parentheses:

$$\log N^f = \sqrt{103} \cdot (1 - S_{dyn}) + \frac{\pi}{2} \cdot (R + \alpha). \quad (5)$$

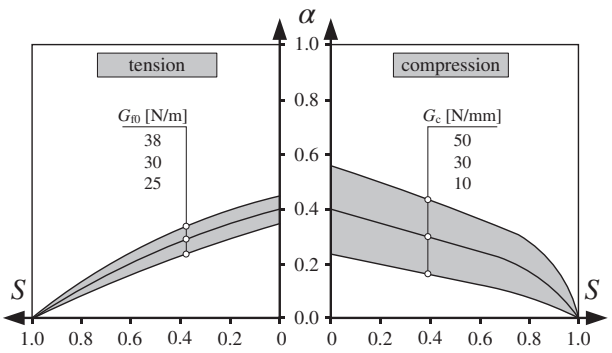

FIGURE 2 Toughness index α for normal strength concrete C 30/37 as a function of stress level and fracture/crushing energy

The underlying experiments cover a parameter range of $0.95 < S < 0.55$; $-0.30 < R < 0.50$; and $f < 20$ Hz and thus include both, pulsating and alternating stresses. Equation (5) applies to normal-strength concrete with and without (subcritical) amounts of steel macrofibres.[24] Ref. 18 contains comprehensive verifications and statistical evaluations of the model uncertainty. Although the SN-α approach is originally derived for uniaxial fatigue it offers possibilities to be enhanced to multiaxial loading conditions, too.

2.2 | Enhancement to multiaxial stress states

The concept behind the extensions is to reduce multiaxial stress conditions to a uniaxial reference state. Thereby, isotropic damage behavior is assumed, so that uniaxial and multiaxial response can be directly combined.

2.2.1 | Basic yield surface formulation

The derivations base on a yield surface formulation originally developed in Ref. 25,26 within the framework of the elasto-plastic continuum damage theory. The yield condition $F(\boldsymbol{\sigma}, \beta_c) \le 0$ is defined by the stress tensor $\boldsymbol{\sigma}$ in the space of effective stresses and combines flow rules according to Drucker-Prager in compression and Rankine in tension. Isotropic material behavior prevails, so that expansions or contractions of the flow surface affect all spatial directions in a same way.[27]

$$F(\sigma,\beta_c) = \frac{1}{1-\alpha_0}\left[q - 3\alpha_0 p + \beta_c\langle\sigma_1\rangle - \gamma\langle-\sigma_1\rangle\right] - \left|\sigma_c\left(\tilde{\varepsilon}^{pl}\right)\right| \le 0 \qquad (6)$$

$$\alpha_0 = \frac{F_{cc}-1}{2F_{cc}-1};\ \beta_c = \frac{\left|\sigma_c\left(\tilde{\varepsilon}^{pl}\right)\right|}{\sigma_t\left(\tilde{\varepsilon}^{pl}\right)}(1-\alpha_0) - (1+\alpha_0),$$

$$\gamma = \frac{3(1-K_c)}{2K_c-1};\ \langle\sigma_1\rangle = \frac{1}{2}(|\sigma_1| + \sigma_1).$$

In Equation (6), the internal memory variable β_c links equivalent plastic strains of the vector $\tilde{\varepsilon}^{pl}$ with uniaxial yield stresses in compression (σ_c) and tension (σ_t), respectively. If these stresses correspond to the uniaxial material strengths, the flow surface reaches its greatest expansion and is referred to as the fracture surface.[19] The dimensionless parameter $F_{cc} = f_{cc}/f_c \ge 1$ describes the relation of uniaxial (f_c) and biaxial (f_{cc}) compressive strengths. K_c is defined within the limits of $0.5 < K_c < 1$ and covers the ratio of the stress invariants on tensile ($\theta = 0°$) and compressive meridians ($\theta = 60°$). Here, the meridian stress states depend on the reference stress according to von Mises q, the hydrostatic stress p and the Lode angle θ.[25,26] They are calculated in the principle stress domain $\hat{\sigma} = (\sigma_1,\sigma_2,\sigma_3)^T$ with $\sigma_1 \ge \sigma_2 \ge \sigma_3$ to

$$q = \sqrt{3J_2}, \qquad (7)$$

$$p = -\frac{1}{3}(\sigma_1+\sigma_2+\sigma_3) = -\frac{1}{3}I_1, \qquad (8)$$

$$\theta = \frac{1}{3}\arccos\left(\frac{3J_3\sqrt{3}}{2J_2^{3/2}}\right), \qquad (9)$$

with

$$J_2 = \frac{1}{6}\left[(\sigma_1-\sigma_2)^2 + (\sigma_2-\sigma_3)^2 + (\sigma_3-\sigma_2)^2\right], \qquad (10)$$

$$J_3 = \left(\sigma_1 - \frac{1}{3}I_1\right)\left(\sigma_2 - \frac{1}{3}I_1\right)\left(\sigma_3 - \frac{1}{3}I_1\right). \qquad (11)$$

In Equation (6), conditional brackets are applied to the maximum principal stress $\langle\sigma_1\rangle$. They represent conditional expressions that enable to cover different shapes of the yield surface due to tension-compression anisotropy within one surface model. In doing so, β_c is activated only if at least one principle stress remains in tension, that is, if $\sigma_1 > 0$. By contrast, γ is exclusively considered in case of triaxial pressure marked by $\sigma_1 < 0$.

2.2.2 | Multiaxial stress level and ratio

In elasto-plastic damage mechanics, the yield condition $F(\boldsymbol{\sigma}, \beta_c) \le 0$ separates linear-elastic stress states ($F < 0$) from those on the yield surface ($F = 0$). This evaluation is realized by converting multiaxial stress states into an equivalent one and comparing it to specific strength criteria. An analogous procedure is used here to define multiaxial stress levels. For this purpose, maximum fatigue stresses of the associated tensor $\boldsymbol{\sigma}_{max}$ are set into relation to the fracture surface ($\sigma_c = f_c$ and $\sigma_t = f_t$), whereat $F = 0$ and material constants α_0, γ according to Equation (6) prevail. Using q^f and p^f as stress invariants of $\boldsymbol{\sigma}_{max}$ according to Equations (7)-(11) and with $\sigma_{max,1}$ as an equivalent principle fatigue stress ($\sigma_{max,1} \ge \sigma_{max,2} \ge \sigma_{max,3}$) the equivalent stress σ_v follows to:

$$\sigma_V = \frac{1}{1-\alpha_0}\left[q^f - 3\alpha_0 p^f + \left(\frac{|f_c|}{f_t}(1-\alpha_0) - (1+\alpha_0)\right)\langle\sigma_{max,1}\rangle - \gamma\langle-\sigma_{max,1}\rangle\right]. \qquad (12)$$

If σ_v is related to the concrete's uniaxial compressive strength, a stress level in multiaxial fatigue arises, namely, S_m that amounts to

$$0 \le S_m = \frac{\sigma_V}{|f_c|} \le 1. \tag{13}$$

Thereby, the application of f_c as a reference strength for σ_V does not go along with any limitations to pure compressive stresses. As both, f_c and f_t are already considered in Equation (12), tensile stresses and mixed stress states of tension-compression alternations are covered as well.[28] However, some restrictions arise due to the underlying material law and the yield surface's open shape. According to Ref. 22, bearing capacities may be overestimated in case of pronounced hydrostatic pressures above $p/f_c > 4$, which, however, usually do not occur at cyclic loadings and thus do not significantly restrict the practical application.

In Figure 3, the previous derivations are exemplarily illustrated using Equation (5) in conjunction with stress levels of Equation (13). For practical application, low stress ratios and low material ductilities are conservatively assumed yielding to $R + \alpha = 0.40$. The shown cyclic fracture surfaces represent multiaxial enhancements of the well known SN curves (cf, Figure 1). They enable to determine logarithmic numbers of cycles to failure for different principal stress states, which are normalized here to the uniaxial compressive strength. As expected due to the assumed damage isotropy, the qualitative shape of the SN surface remains unchanged even at different stress levels.

To additionally cover the frequency effect, an equivalent stress ratio at the minimum fatigue stress $S_m(\boldsymbol{\sigma}_{min})$ has to be derived first using the associated stress tensor $\boldsymbol{\sigma}_{min}$ instead of $\boldsymbol{\sigma}_{max}$. The mean stress velocity $\dot{\sigma}_{m,m}$ is then approximated by

$$\dot{\sigma}_{m,m} = |S_m(\sigma_{max}) \cdot f_v - S_m(\sigma_{min}) \cdot f_v| \cdot f \cdot \alpha_{F-t}, \tag{14}$$

whereas

$$f_v = \begin{cases} f_t, \text{if } \sigma_{max,1} \cdot f_t^{-1} \ge |\sigma_{max,3} \cdot f_c^{-1}| \\ f_c, \text{if } \sigma_{max,1} \cdot f_t^{-1} < |\sigma_{max,3} \cdot f_c^{-1}| \end{cases}, \tag{15}$$

serves to distinguish between predominantly compressive or tensile stresses. Compression and thus f_c as the quasi-static reference strength f_v governs, if the ratio of the maximum fatigue stress at the upper load level $\sigma_{max,1}$ to the quasi-static tensile strength f_t is smaller than the ratio of the minimum fatigue stress $\sigma_{max,3}$ to the compressive strength f_c. Otherwise, tension and $f_v = f_t$ dominates. The dynamic stress level $S_{m,dyn}$ finally follows analogous to Equation (3) and R_m as a corresponding stress ratio equivalent to Equation (2).

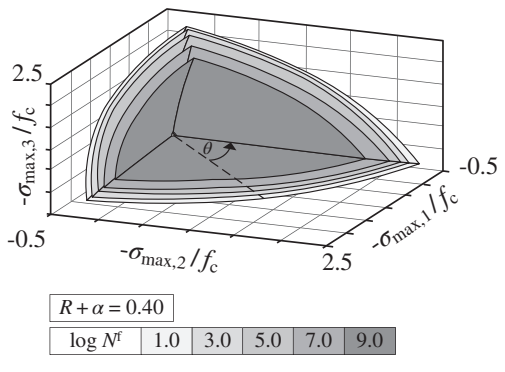

FIGURE 3 SN curves for multiaxial stress states

$$S_{m,dyn} = \frac{S_m}{\left[\frac{\dot{\sigma}_{m,m}}{\dot{\sigma}_0}\right]^c} \tag{16}$$

$$R_m = \frac{S_m(\sigma_{min}) \cdot f_v}{S_m(\sigma_{max}) \cdot f_v} \tag{17}$$

2.3 | Verification

Test results taken from the literature[11,29–33] serve to verify the approach. Table 1 summarizes the main data, which comprise multiaxial fatigue in compression (C), tension (T) and with alternating stresses of tension and compression (TC). Biaxial (2D) and triaxial (3D) compression as well as biaxial tension-compression fields are covered. S_m, R_m, and f encompass the mentioned parameter ranges and thus represent load conditions of practical relevance. Experimental load-time functions are always sinusoidal yielding to $\alpha_{F-t} = 2$. For recalculations, the compressive strength increase due to radial reinforcement in Ref. 29 is mathematically captured applying the equations provided in Ref. 17.

As detailed information on the postcracking, quasi-static load-deformation behavior of the reference specimens are not available in Ref. 11,29–33, the toughness index is assumed here to a constant value of $\alpha = 0.20$ for simplicity. This procedure is rather conservative for compressive fatigue, as the strength-increasing effect of multiaxial compared to uniaxial stresses gives advice for an analogous increase in ductility. The material parameters $F_{cc} = 1.16$ and $K_c = 0.66$ are taken as proposed in Ref. 22,23.

Figure 4 compares calculated and experimental numbers of cycles to failure (subscript calc and test) in logarithmic scale. Appropriate mathematical estimates are thus located on the central diagonal of the scatter plot. Despite of the large inherent scatter of experimental fatigue data,[1,3,4,7] the results agree quite well on average with a slight tendency towards a mathematical underestimation. Thus, the results tend to lie above the diagonals, what however applies to a lesser extent to triaxial compression (Figure 4A) than to biaxial compression (Figure 4B) and mixed states of tension-compression (Figure 4C).

2.4 | Design chart

Figure 5 illustrates the derived equations for biaxial loadings with $R + \alpha = 0.40$ and $f < 1$ Hz, that is, conservatively for brittle concretes and low stress rates and velocities. Principle fatigue stresses $\sigma_{max,1}$ and $\sigma_{max,2}$ are normalized to the uniaxial compressive strength f_c and SN curves are drawn for different fatigue lifes. The cyclic fracture

TABLE 1 Multiaxial fatigue tests taken from the literature

Denomination	Reference	Stress state	S_m	R_m	f (Hz)
Hooi-2000	29	C (3D)	0.95; 0.65	0.02	1
Takhar-1974	30	C (2D)	0.90; 0.71	0.20; 0.25	20; 60
Traina-1982	31	C (2D)	0.98; 0.55	0	1
Wang-2011	11	T,C,TC (2D)	0.91; 0.53	–0.40; 0.35	1
Yin-1995	32	C (2D)	0.99; 0.59	0.05	1
Zhu-2003	33	C (2D)	0.82; 0.51	0.10	5

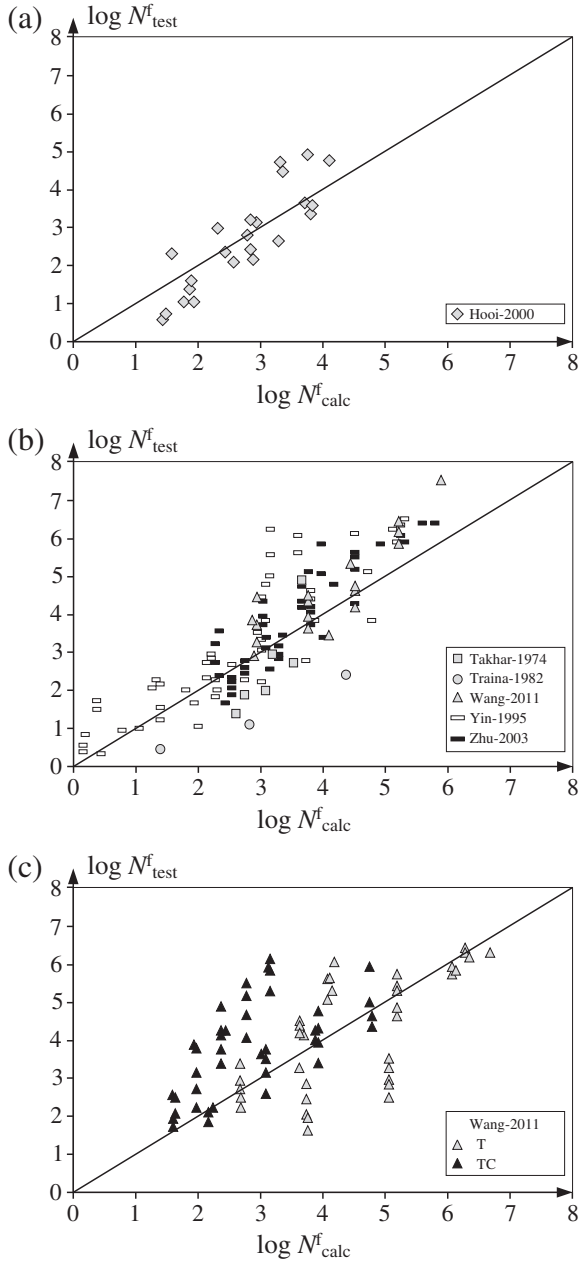

FIGURE 4 Comparison with calculated (calc) and experimental (test) numbers of cycles to failure N^f for (A) triaxial compression, (B) biaxial compression, and (C) biaxial tension and tension-compression

surface marked with log N^f = 1 corresponds to that at quasi-static loadings. It fits well to the so-called Kupfer curves for biaxial strengths[34] proving a high accuracy of the approach and a direct connection to well established quasi-static failure surfaces.

In Figure 5, intermediate values of log N^f might be linearly interpolated for various stress conditions. In case of deviating toughness indexes (Figure 2), stress ratios or frequencies, Equations (5) to (17) apply.

3 | ACCUMULATION OF DAMAGE AT MULTISTAGE LOADINGS

3.1 | Determination of load packages

SN curves usually base on constant amplitude tests under laboratory conditions. However, existing structures under operating conditions are often exposed to multistage loadings with variable frequencies, stress levels and amplitudes that exhibit more or less random sequences of loading and unloading over time. As SN curves do not enable to directly determine fatigue lifes for multistage loading processes, refined methods are necessary. Here, a three step strategy is proposed. At first, relevant informations like maximum and minimum stresses within hysteretic loops are recorded with suitable counting methods like the Rainflow approach (Figure 6A and 6B). Second, decisive output is extracted, classified into groups (load packages) and processed by empirical probability density functions (pdf, Figure 6C).

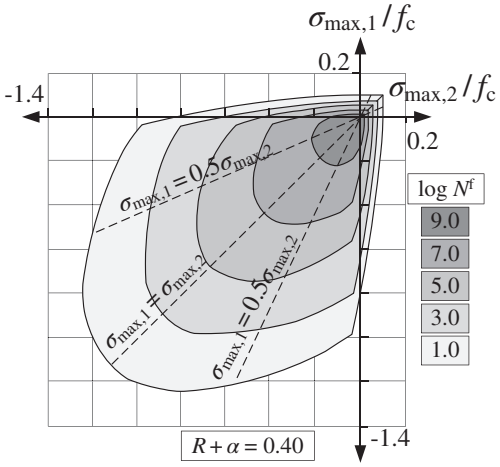

FIGURE 5 Wöhler-surface for biaxial stress states

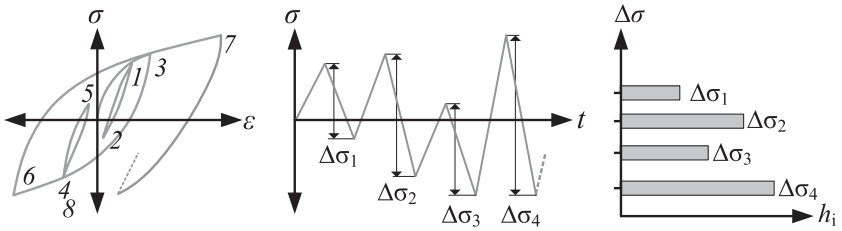

(a) hysteretic loops (b) Rainflow-approach (c) density function

FIGURE 6 Recording and statistical evaluation of variable amplitude cyclic loads according to Refs. 1,35

The resulting cumulative density function (cdf) is referred to as the stress or load spectrum.[35] However, it does no longer contain information on time dependencies like the sequence of loading and unloading. Third, the cdfs are used to determine and accumulate the amount of damage caused per individual load package. For this purpose, the Palmgren-Miner rule, often just called Miner's rule, is well established. It introduces a nondimensional damage variable D that sums damage increments from $D = 0$ at an initial state to $D = 1$ at the calculative failure.[36–38]

3.2 | Palmgren-Miner hypothesis

The Palmgren-Miner rule[39,40] linearly accumulates damage portions. Total damage D follows from a load package consisting of j groups by summing up all individual components D_i. Each portion D_i is determined relating the number of applied loading cycles N_i to the associated number of cycles to failure N^f_i according to the SN approach. D then results to:

$$D = \sum_{i=1}^{j} D_i = \sum_{i=1}^{j} \frac{N_i}{N_i^f} \leq 1. \tag{18}$$

Regardless of the loading sequence, relative damage contributions are uniquely assessed via the material's resistances at constant amplitude fatigue. According to the shape of the underlying SN curve, high stress levels contribute far more to the total damage than low ones. However, experiments with variable stress amplitudes prove that fatigue fracture occurs at Miner sums that may even noticeably deviate from $D = 1$.[35,41] Moreover, it is recognized that the sequential arrangement of loadings takes influence on the fatigue resistance.

In a two-staged loading process with decreasing ($S_1 > S_2$) or increasing ($S_1 < S_2$) stress levels over time, $N_{2,res}$ denotes the number of loading cycles that can be endured at S_2 up to failure. According to Palmgren-Miner, $N_{2,res}$ is obtained by rearranging Equation (18) into

$$\frac{N_1}{N_1^f} + \frac{N_{2,res}}{N_2^f} = 1 \Longrightarrow N_{2,res} = \left(1 - \frac{N_1}{N_1^f}\right) N_2^f. \tag{19}$$

During the tests in Ref. 42, the change from a high to a low stress level (unloading) yields to an increase in the residual number of cycles $N_{2,res}$ compared with Equation (19) and vice versa. The authors in Refs. [43,44] report on similar observations, although to a less extent. By contrast, results in Refs. 45,46 show reduced fatigue lifes with unloading and vice versa. However, as the experimental basis is still rather limited, the data do not appear representative.

If prognoses according to Equation (18) or derivatives published in the scientific literature[3,8,41] are verified to experimental data, they agree well only on average of loading and unloading or in case of specific loading sequences.[47] For more realistic predictions and a generalized approach, magnitude and point of time of stress changes have to be taken into account, too.

3.3 | Modified accumulation model

The basic idea behind the presented approach is to use the achieved material damage state as a transfer parameter between distinct loading packages. Thereby, damage is defined as the loss of initial stiffness, so that $0 < d \leq 1$ describes the ratio of degraded (E^f_c) to initial (E_c) elastic stiffness (cf, Figure 7. The value of d increases over time ($\dot{d} \geq 0$) and thus healing recoveries are impossible.

According to the envelope concept[3,8] and due to the mechanical basis, fatigue fracture usually occurs in constant amplitude fatigue at ultimate damage states of $d < 1$.[45–49] The evolution of damage over time corresponds well to s-shaped creep curves[50] and results in enhanced damages with decreasing stress levels. Related sets of curves showing damage as a function of stress level and related numbers of cycles to failure $0 \leq n = N/N^f \leq 1$ are shown in Figure 8 or can be taken from Ref. 18. While $n = 0$ marks the initial state, $n = 1$ corresponds to failure with $N = N^f$. Due to the monotonously increasing shape ($\partial d/\partial n \geq 0$, no recovery of stiffness due to crack closure), distinct relations between d and n occur. However, correlations between the damage parameter d and the counting variable D do not yet exist.

As test results in Ref. 48 prove a continues evolution of damage over time, stress level changes theoretically require to mathematically adapting the numbers of cycles to failure N^f according to the SN approach. The modification is not covered by the Palmgren-Miner rule and thus leads to a new damage accumulation approach. Figure 8 illustrates its basics with the example of a two-stage loading process. It considers two damage evolutions $d_1(S_1)$ and $d_2(S_2)$ from the stress levels S_1 and S_2 and intermediate changes between the curves. If stress level changes after N_1 cycles, a damage state $d_{1/2}$ has to be transferred. It is associated with related numbers of cycles $n_1(S_1)$ and $n_2(S_2)$, respectively. As $N_1/N^f{}_2 \neq n_2$, the cycle number $N^f{}_2$ according to the SN approach has to be modified to $N_2{}^{f,mod}$ by

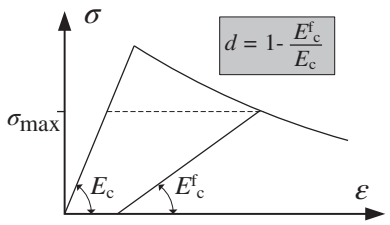

FIGURE 7 Definition of the damage variable d

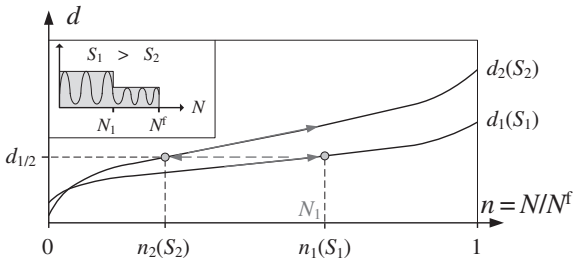

FIGURE 8 Concrete damage evolution in fatigue for different stress levels S_1 and S_2

$$N_2^{f,mod} = \frac{N_1}{n_2(S_2)}. \tag{20}$$

The residual numbers of cycles $N_{2,res}$ assigned to S_2 follow in dependence on Equation (19).

$$N_{2,res} = \left(1 - \frac{N_1}{N_2^{f,mod}}\right) \cdot N_2^f. \tag{21}$$

Thus, $N^f = N_1 + N_{2,res}$ load cycles are endurable in total. The procedure can be generalized to arbitrarily multistage fatigue by always investigating two successive loading packages S_i and S_{i+1}. The accumulation of N/N^f is then carried out similar to Equation (18) using the parameter D.

$$D = D_i + \Delta D_{i+1} = \sum_i \frac{N_i(S_i)}{N_i^f(S_i)} + \frac{N_{i+1}(S_{i+1})}{N_{i+1,res}(S_{i+1})} \cdot [1 - n_i] \le 1. \tag{22}$$

It should be noted that the accumulation requires expensive determinations and evaluations of damage evolutions over time $d(n)$. Thus, a simplified approach is proposed subsequently. Both methods can be used alternatively and provide almost identical fatigue lifes.

3.3.1 | Approximation

If stress levels change from S_i to S_{i+1} at a cycle time $n_i = N_i(S_i) / N_i^f(S_i)$ with an accumulated damage state D_i, the residual numbers of cycles assigned to S_{i+1} follow to

$$N_{i+1,res}(S_{i+1}) = \varphi_{i+1} \cdot N_{i+1}^f(S_{i+1}). \tag{23}$$

Here, N^f_{i+1} denotes the numbers of cycles to failure that result for the stress level S_{i+1} applying Equation (5). They are multiplied by a nondimensional weighting function $\varphi(n_\varphi, \xi)$ defined in the interval of $0 < \varphi \le 1$ according to Equation (24), to evaluate effects of the point in time (via n_φ and Equation [25]) and the magnitude of a stress change (via ξ and Equation [26]) on residual fatigue lifes.

$$\varphi_{i+1} = \begin{cases} \frac{-1}{2n_\varphi} n_i + 1 & \text{for } 0 \le n_i \le n_\varphi \\ \frac{1}{2(n_\varphi - 1)} (n_i - 1) & \text{for } n_\varphi \le n_i \le 1 \end{cases}. \tag{24}$$

$$n_\varphi = 0.5\xi + 0.5;\ 0 \le n_\varphi \le 1. \tag{25}$$

$$\xi = \langle S_i - S_{i+1} \rangle^\beta - \langle S_{i+1} - S_i \rangle^\beta;\ \beta > 0;\ -1 \le \xi \le 1. \tag{26}$$

The exponent $\beta > 0$ determines the stress difference between S_i and S_{i+1}, whereby the conditional brackets distinguish between loading and unloading. Load increases $S_i < S_{i+1}$ result in $\xi < 0$, unloading $S_i > S_{i+1}$ in $\xi > 0$. In the intermediate case $S_i = S_{i+1}$, a value of $\xi = 0$ arises. Generally, increased values of β yield to reduced amounts of ξ, which, in case of $\xi = 0$, trace the equations back to Palmgren-Miner's linear rule. Hence, low values of the weighting parameter β are favored. They tend to $|\xi| \to 1$ as illustrated in Figure 9 and lead to a strong consideration of sequence effects in nonlinear damage accumulations even in case of low stress level changes.

3.4 | Verification to experimental data

The test results of two-stage loading processes with loading and unloading according to Hilsdorf and Kesler[42] serve for model verifications. Figure 10 shows the investigated loading sequences and related values of cycles. Thereby, model predictions according to Equation (22) are represented by solid lines, those according to Palmgren-Miner (PM) by dashed lines and experimental data by single points. White points refer to load combination (LC) 1 (loading), gray ones to LC 2 (unloading). For recalculations, a concrete of strength class C 30/37 with $S = 0.40$ or $S = 0.80$ and $R = 0$ is assumed. β is set equal to 0.1 as advised by Ref. 18.

As expected, the linear Palmgren-Miner rule only provides accurate predictions on average, not covering any effects of sequence. By

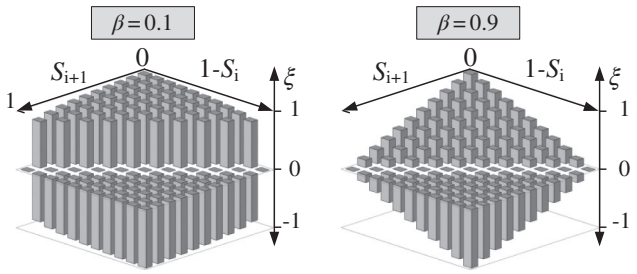

FIGURE 9 Effect of β on the weighting factor of the stress difference ξ

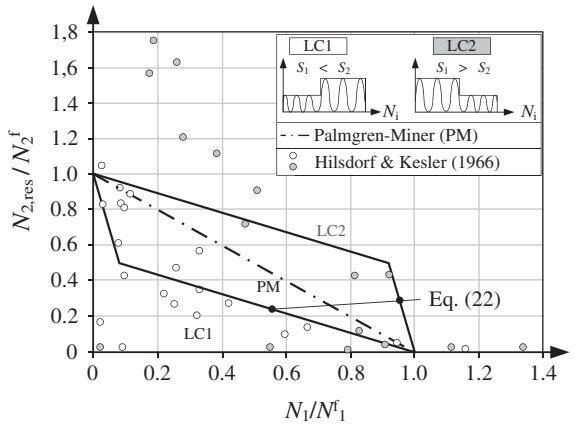

FIGURE 10 Residual numbers of cycles to failure in two-stage loading process

contrast, the nonlinear approach of Equation (22) accurately depicts reduced values $N_{2,res}$ due to load increases. However, the experimentally suggested increase in fatigue lifes above $N_{2,res} / N^f_2 > 1$ and thus above the numbers of cycles to failure in case of constant amplitude fatigue cannot be mapped by the model. As these effects may only occur due to consolidations within the concrete's matrix[3,8] and as a consequence of unloading within the early phase of fatigue life ($N_1/ N^f_1 < 0.3$), its neglection stays on the safe side for a cross-sectional design.

Table 2 summarizes the main material and model parameters used in the article and their sources in literature.

4 | EXAMPLE

The application of the developed model is demonstrated using the example of a triaxial and three-stage loading process. The aim is to show that fatigue lifes increase, if unloading occurs. This holds true for uniaxial loadings as well as multiaxial ones and can only be captured by nonlinear damage accumulation.

A concrete of strength class C 30/37 with uniaxial compressive and tensile strengths of f_c = 38 N/mm^2 and f_t = 2,9 N/mm^2 is assumed. Basically, the principle stresses of the triaxial loading situation consist of one tensile stress σ_1 = 1 MPa and two compressive ones σ_2 = −10 MPa and σ_3 = −25 MPa, which are summarized within the fatigue stress vector $\boldsymbol{\sigma}_j$ = [1-10 -25]^T, j = max and min, respectively. The change at maximum and minimum load level as well as in dependence on the i = 1, 2, 3 constant amplitude load packages is described by the loading factor λ^i_j resulting in $\lambda^i_j \cdot \sigma_j$. Here, load changes from the first to the second package occur after log $N_{1/2}$ = 2.0 cycles, those from the second to the third after in total log $N_{2/3}$ = 2.5 cycles. The number of cycles to failure N^f is in question and should be estimated with the derived model. Table 3 briefly summarizes the main steps of the calculation.

TABLE 2 Material and model parameters for fatigue lifetime assessment of concrete in case of multiaxial and multistage loadings

Parameter	Value	Equation	Source
K_c	0.66	(6), (12)	22,23
F_{cc}	1.16	(6), (12)	22,23
α	0 to 0.35 (brittle concrete) 0 to 0.55 (ductile concrete) 0 to 0.90 (steel fiber reinforced concrete)	(5)	Figure 2 16
$\alpha_{F\text{-}t}$	1 (rectangular waveform) 2 (sinusoidal waveform)	(5)	13,16
c	0.0158	(3)	17,28
β	0.1	(26)	18

The calculative fatigue failure associated with D = 1 occurs after N^f = 104.402 + 316 = 104.718 cycles and thus much later than predicted by Palmgren-Miner with N^f = 91.614. The difference in lifetime amounts here to 14.3% and is caused by unloading effects. Thus, the new history-dependent damage accumulation approach provides benefits in terms of economic design results.

5 | CONCLUSIONS

In the article, the effect of multiaxial and multistage loadings on the fatigue performance of normal-strength concrete is investigated and modeled via novel, mechanically based approaches. At first, relevant fatigue parameters are identified, which is stress level as the ratio of maximum fatigue stress and concrete's strength, stress ratio as the quotient of minimum and maximum fatigue stress, loading frequency, and material ductility. In cases of variable amplitude loadings, related numbers of cycles to stress changes as well as sequence and magnitude of loading and unloading have to be taken into account, too.

To enhance established SN approaches for uniaxial fatigue to arbitrary multiaxial conditions, an equivalent stress is introduced. It relies on a yield surface formulation of elasto-plastic continuum damage mechanics and transfers multiaxial stress conditions into a uniaxial reference state. The reference state serves to compute appropriate stress levels and ratios, whereby compression, tension and mixed configurations of tension-compression are covered. The equations are elaborated to a design chart for biaxial loading conditions and verified to experimental data taken from the literature. Both, model predictions and test results agree well on average.

To further extend the model to multistage loadings, a mechanically based damage accumulation procedure is developed. It modifies the linear approach of Palmgren-Miner with respect to the loading sequence. Loading and unloading, which lead to previously unconsidered reductions or increases of residual numbers of cycles to failure are now taken into account. For this purpose, the inner damage variable of stiffness reduction is used as a transfer parameter between individual loading packages. It evaluates the effect of both, numbers of cycles until stress change and its magnitude. The new approach is verified to experimental data and agrees well on average. However, effects of unloading in the early stage of fatigue life, which in experiments give rise to enhanced fatigue lifes due to the consolidation of

TABLE 3 Example for a fatigue lifetime analysis in case of multiaxial and multistage loadings

		Load package 1		Load package 2		Load package 3	
		λ^1_{max}	λ^1_{min}	λ^2_{max}	λ^2_{min}	λ^3_{max}	λ^3_{min}
Parameter	**Equation**	**1.0**	**0.2**	**0.8**	**0.3**	**0.7**	**0.1**
S_m	(13)	0.865	0.173	0.692	0.259	0.605	0.086
σ_m/σ_0	(14)	262.9		164.3		197.2	
f_v (MPa)	(15)	−38		−38		−38	
$S_{m,dyn}$	(16)	0.792		0.638		0.557	
R_m	(17)	0.200		0.375		0.143	
α	Figure 2	0.123		0.196		0.230	
$\log N^f$	(5)	2619		4568		5083	
D_i	(22)	0.240		0.246			
ξ	(26)	0.829		0.778			
η_ϕ	(25)	0.915		0.889			
ϕ_i	(24)	0.869		0.862			
$N_{i,\,res}$	(23)	32.132		104.402			

mortar, cannot be predicted. The model underestimates those increases, which lies on the safe side for cross-sectional designs.

ORCID

Peter Heek https://orcid.org/0000-0002-3304-2501

REFERENCES

1. König G, Danielewicz I. *Ermüdungsfestigkeit von Stahlbeton- und Spannbetonbauteilen mit Erläuterungen zu den Nachweisen gemäß CEB-FIB Model Code 1990*. Deutscher Ausschuss für Stahlbeton (DAfStb), Heft. Volume 439. Berlin: Beuth Verlag, 1994.
2. Tepfers R. Tensile fatigue strength of plain concrete. ACI J. 1979;76 (39):919–933.
3. Shah P. Fatigue of concrete structures. Detroit: ACI-Publication SP-75, 1982.
4. Hsu TTC. Fatigue of plain concrete. ACI J. 1981;78(4):292–305.
5. Aas-Jakobsen, K.: *Fatigue of concrete beams and columns*. Bulletin No. 70–1, Division of Concrete Structuresm Trondheim, 1970.
6. Cornelissen HAW, Reinhardt HW. Uniaxial tensile fatigue failure of concrete under constant amplitude and programme loading. Mag Concr Res. 1984;36(129):216–226.
7. Zhang B, Phillips DV, Wu K. Effects of loading frequency and stress reversals on fatigue life of plain concrete. Mag Concr Res. 1996;48 (177):361–375.
8. Mallet, G.: Fatigue of reinforced concrete, State of the art review/2. Transport and Road Research Laboratory (TRRL), London, 1991.
9. Award, M.E.; Hilsdorf, H.K. *Strength and deformation characteristics of plain concrete subjected to high repeated and sustained loads*. Urbana, No. 372, University of Illinois, 1971.
10. Nelson EL, Carrasquillo RL, Fowler DW. Behaviour and failure of high-strength concrete subjected to biaxial-cyclic compression loading. ACI Mater J. 1988;85(4):248–253.
11. Wang HL, Song YP. Fatigue capacity of plain concrete under fatigue loading with constant confined stress. Mater Struct. 2011;44(1): 253–262.
12. Lohaus L, Wefer M, Oneschkow N. Ermüdungsbemessungsmodell für normal-, hoch- und ultrahochfeste Betone. Beton- und Stahlbetonbau. 2011;106(12):836–846.
13. Schneider S, Vöcker D, Marx S. Zum Einfluss der Belastungsfrequenz und der Spannungsschwingbreite auf die Ermüdungsfestigkeit von Beton. Beton- und Stahlbetonbau. 2012;107(12):836–845.
14. Oneschkow N. In: Leibniz Universität Hannover, editor. Analyse des Ermüdungsverhaltens von Beton anhand der Dehnungsentwicklung. Dissertation, Leibniz Universitat Hannover, 2014.
15. Elsmeier K, Hümme J, Oneschkow N, Lohaus L. Prüftechnische Einflüsse auf das Ermüdungsverhalten hochfester feinkörniger Vergussbetone. Beton- und Stahlbetonbau. 2016;111(4): 233–240.
16. Heek P, Mark P. Zur Ermüdung von Beton und Stahlfaserbeton. Beton- und Stahlbetonbau. 2016;111(4):221–232.
17. CEB-FIB. Model Code 90. Thomas Telford, 1993.
18. Heek P. Modellbildung und numerische Analysen zur Ermüdung von Stahlfaserbeton. Dissertation, Ruhr-Universität Bochum, 2017.
19. Mark P. Zweiachsig durch Biegung und Querkräfte beanspruchte Stahlbetonträger. Habilitation, Ruhr-Universität Bochum, 2006.
20. Hillerborg A. Analysis of crack formation and crack growth in concrete by means of fracture mechanics and finite elements. Cem Concr Res. 1976;6(6):773–781.
21. Anders S. Betontechnologische Einflüsse auf das Tragverhalten von Grouted Joints. Dissertation. Leibniz Universität Hannover, 2007.
22. Vonk RA. A micromechanical investigation of softening of concrete loaded in compression. Heron. 1993;38(3).
23. Gödde L, Mark P. Numerical simulation of the structural behaviour of SFRC slabs with or without rebar and prestressing. Mater Struct. 2015;48(6):1689–1701.
24. Heek P, Tkocz J, Mark P. A thermo-mechanical model for SFRC beams or slabs at elevated temperatures. Mater Struct. 2018;51(87).
25. Lubliner J, Oliver J, Oller S, Onate E. A plastic-damage model for concrete. Int J Solids Struct. 1989;25(3):299–326.
26. Lee J, Fenves GL. Plastic-damage model for cyclic loading of concrete structures. J Eng Mech. 1998;124(8):892–200.
27. Chen WF. Plasticity in reinforced concrete. New York: McGraw-Hill Book Company, 1982.
28. Heek, P.; Mark, P: Numerical simulation of steel fibre reinforced concrete girders subjected to cyclic loads. In: D.A. Hordijk, D.A.; Lukovic, M. (Eds.), Proc. 2017 fib symposium high tech concrete:

Where technology and engineering meet, Netherlands, 2017, pp. 356–365.
29. Hooi TT. Effects of passive confinement on fatigue properties of concrete. Mag Concr Res. 2000;52(1):7–15.
30. Takhar SS, Jordaan IJ, Gamble BR. Fatigue of concrete under lateral confining pressure. ACI Spl Pub. 1974;SP-41:59–69.
31. Traina LA, Jeragh AA. Fatigue of plain concrete subjected to biaxial-cyclic loading. ACI Spl Pub. 1982;SP-75:217–233.
32. Yin W, Hsu TTC. Fatigue behaviour of steel fibre reinforced concrete under uniaxial and biaxial compression. ACI Mater J. 1995;92 (1):1–11.
33. Zhu J-S, Song Y-P, Cao W. Fatigue behaviour of plain concrete under biaxial compression. Chin Ocean Eng. 2003;17(4):617–630.
34. Grübl P, Weigler H, Karl S. Beton-Arten, Herstellung und Eigenschaften. Springer Verlag, 2001.
35. Zilch K, Zehetmaier G. Bemessung im konstruktiven Ingenieurbau. Berlin: Springer Verlag, 2010.
36. Sanio D, Löschmann J, Mark P, Ahrens MA. Bauwerksmessungen versus Rechenkonzepte zur Beurteilung von Spannstahlermüdung in Betonbrücken. Bautechnik. 2018;95(2):99–110.
37. Sanio D, Ahrens MA, Rode S, Mark P. Untersuchung einer 50 Jahre alten Spannbetonbrücke zur Genauigkeitssteigerung von Lebensdauerprognosen. Beton- und Stahlbetonbau. 2014;109(2):128–137.
38. Ahrens MA, Mark P. Lebensdauersimulationen von Betontragwerken - Stochastische Strukturberechnungen über die Zeit am Beispiel einer gealterten Bogenbrücke. Beton- und Stahlbetonbau. 2011;106(4): 220–230.
39. Palmgren A. Die Lebensdauer von Kugellagern. Zeitschrift Verein Deutscher Ingenieure. 1924;58:339–341.
40. Miner MA. Cumulative damage in fatigue. J Appl Mech. 1945;67: 159–164.
41. Grzybowski M, Meyer C. Damage accumulation in concrete with and without fibre reinforcement. ACI Mater J. 1993;90(6):594–604.
42. Hilsdorf HK, Kesler CE. Fatigue strength of concrete under varying flexural stresses. ACI J. 1966;63(10):1059–1076.
43. Hordijk DA. Tensile and tensile fatigue behaviour of concrete: Experiments, modelling and analyses. Heron. 1992;37(1).
44. Klausen D. Festigkeit und Schädigung von Beton bei häufig wiederholter Beanspruchung. Dissertation, TH Darmstadt, 1978.
45. Holmen, J.O.: Fatigue of concrete by constant and variable amplitude loading. PhD-Thesis, The Norwegian Institute of Technology, Trondheim, 1979.
46. Baktheer A, Camps B, Hegger J, Chudoba R. Numerical and experimental investigations of concrete fatigue behaviour exposed to varying loading ranges, fib congress. Melbourne, 2018.
47. Heek P, Ahrens MA, Mark P. Incremental-iterative model for time-variant analysis of SFRC subjected to flexural fatigue. Mater Struct. 2017;50(62):1–15.
48. Göhlmann, J.: Zur Schädigungsberechnung an Betonkonstruktionen für Windenergieanlagen unter mehr-stufiger und mehraxialer Ermüdungsbeanspruchung. Dissertation, Leibniz Universität Hannover, 2009.
49. Pfanner D. In: Ruhr-Universität Bochum, editor. Zur Degradation von Stahlbetonbauteilen unter Ermüdungsbeanspruchung. Dissertation, 2002.
50. Nakov D, Markovski G, Arangjelovski T, Mark P. Experimental and analytical analysis of creep of steel fibre reinforced concrete. Period Polytech Civil Eng. 2018;62(1):226–231.

How to cite this article: Heek P, Mark P. Multiaxial and variable amplitude fatigue of concrete. *Civil Engineering Design*. 2019;1:87–96. https://doi.org/10.1002/cend.201900010